Sign-problem-free quantum Monte Carlo
of the onset of antiferromagnetism in metals[*]

Erez Berg,[1,2*] Max A. Metlitski,[3] Subir Sachdev[1,4]

[1]Department of Physics, Harvard University, Cambridge MA 02138, USA
[2]Department of Condensed Matter Physics, Weizmann Institute of Science, Rehovot 76100, Israel
[3]Kavli Institute for Theoretical Physics, University of California, Santa Barbara, CA 93106, USA
[4]Instituut-Lorentz for Theoretical Physics, Universiteit Leiden,
P.O. Box 9506, 2300 RA Leiden, The Netherlands

[*]To whom correspondence should be addressed; E-mail: erez.berg@gmail.com.

The quantum theory of antiferromagnetism in metals is necessary for our understanding of numerous intermetallic compounds of widespread interest. In these systems, a quantum critical point emerges as external parameters (such as chemical doping) are varied. Because of the strong coupling nature of this critical point, and the "sign problem" plaguing numerical quantum Monte Carlo (QMC) methods, its theoretical understanding is still incomplete. Here, we show that the universal low-energy theory for the onset of antiferromagnetism in a metal can be realized in lattice models, which are free from the sign problem and hence can be simulated efficiently with QMC. Our simulations show Fermi surface reconstruction and unconventional spin-singlet superconductivity across the critical point.

The presence of an antiferromagnetic transition in a metal is common to compounds such as electron-doped cuprates (*1*), iron based superconductors (*2*), and heavy fermion Kondo lattice systems (*3*). Whereas our understanding of quantum antiferromagnetism in insulators has seen remarkable advances (*4*), analogous problems in metals are far more complicated because of the subtle interplay between the low energy fermionic quasiparticles on the Fermi surface, and the quantum fluctuations of the antiferromagnetic order parameter. In addition, the presence of the Fermi surface has hampered large scale numerical studies, because QMC algorithms are afflicted by the well-known fermion sign problem. Such algorithms express the partition function as a sum over Feynman histories, and the sign problem arises when the weights assigned to the trajectories are not all positive because of quantum interference effects. A general solution to the fermion sign problem has been proved to be in the computational complexity class of nondeterministic polynomial (NP) hard (*5*), and so there has been little hope that the antiferromagnetic quantum critical point could be elucidated by computational studies.

Application of the methods of quantum field theory and the renormalization group to the onset of antiferromagnetism in a metal (*6*), has identified (*7, 8*) a universal quantum field theory which captures all the singular low energy quantum fluctuations that control the quantum critical point and deviations from the Fermi liquid physics of traditional metals. In two spatial dimensions, the field theory is expressed in terms of fermionic excitations in the vicinity of a finite number of 'hot spots' on the Fermi surface, and is thus independent of the details of the fermionic band-structure, except for the number of hot-spots and Fermi-velocities at the hot-spots (*9*). Recent work (*10, 11*) has shown that the renormalization group and Feynman graph expansions of the field theory flow to strong coupling, making further analytical progress difficult.

Here, we show that the universal quantum field theory can be realized in lattice models which are free of the sign problem, and so is amenable to large scale QMC studies. Our claim

does not contradict the no-go theorem of Ref. (5), because we do not provide a general recipe for eliminating the sign problem. However, we will eliminate it for the specific case of the onset of antiferromagnetic order in a two-dimensional metal, provided the perturbative arguments on the importance of the hot spots to the quantum field theory (7, 8, 10, 11) apply. Our modified lattice model has at least two bands. Therefore, in cases in which there is only a single active band at the transition, such as in the electron-doped cuprates, our method requires modifying Fermi surface far away from the hot spots; we show that this can be done while preserving the universal low-energy properties of the antiferromagnetic critical point. On the other hand, our method applies to multi-band situations (such as in the iron-based superconductors) without changes to their Fermi surface configuration. Being a low-energy effective theory, the method will not apply where the proximity of a Mott insulator is important, as is likely the case in the hole-doped cuprates (12–16).

To illustrate our method, we now consider the onset of antiferromagnetic order in a simple one-band model on the square lattice, as is appropriate for the electron-doped cuprates. The electrons, $c_{\mathbf{k}}$ (the spin index is left implicit), with dispersion $\varepsilon_{\mathbf{k}}$, have a single "large" Fermi surface (Fig 1A). The antiferromagnetic order parameter is $\vec{\varphi}_{\mathbf{q}}$; we will assume the important fluctuations of $\vec{\varphi}_{\mathbf{q}}$ are restricted to small values of $|\mathbf{q}|$, much smaller than the size of the Brillouin zone. The antiferromagnetic ordering wavevector is $\mathbf{K} = (\pi, \pi)$, and $\vec{\varphi}_{\mathbf{q}}$ represents the electron spin density at the wavevector $\mathbf{K} + \mathbf{q}$; we will also refer to the antiferromagnetic order as spin density wave (SDW) order. We can now write the electron part of the Hamiltonian as

$$H = \sum_{\mathbf{k}} \varepsilon_{\mathbf{k}} c_{\mathbf{k}}^{\dagger} c_{\mathbf{k}} + \lambda \sum_{\mathbf{k},\mathbf{q}} c_{\mathbf{k}+\mathbf{K}+\mathbf{q}}^{\dagger} \left(\vec{s} \cdot \vec{\varphi}_{\mathbf{q}} \right) c_{\mathbf{k}} \tag{1}$$

where λ is the 'Yukawa' coupling between the electrons and the SDW order, and $\vec{s}$ are the Pauli matrices. The Yukawa term is the simplest coupling consistent with translational symmetry and spin-rotation invariance, and can be derived *e.g.* by decoupling of the repulsive interaction in a

Hubbard model by an auxiliary field which maps to $\vec{\varphi}$ in the long-wavelength limit (*17*). The hot spots are at $\mathbf{k}$ for which $\varepsilon_{\mathbf{k}} = \varepsilon_{\mathbf{k+K}} = 0$ (Fig. 1A); at these points, $\vec{\varphi}_{\mathbf{q}=0}$ scatters electrons between initial and final states which are both on the Fermi surface. To obtain the electron Fermi surface in a metal with SDW order, we replace $\vec{\varphi}_{\mathbf{q}}$ by its expectation value $\langle \vec{\varphi}_q \rangle = \vec{N} \delta_{\mathbf{q},0}$ (where $\vec{N}$ is the staggered magnetization), and recompute the electron dispersion; this leads to the Fermi surface reconstruction shown in Fig. 1B.

We now describe our method to deform the model, such that the sign problem is avoided, while preserving the structure of the hot spots. Let us separate the hot spots into two groups, so that $\mathbf{K}$ only connects hot spots from one group to the other. Now deform the one-band electronic dispersion to a two-band model with an additional 'orbital' label, so that all the hot spots in one group are on the Fermi surfaces of the first band, while the hot spots of the other group reside on the Fermi surfaces of the second band (an example of such a dispersion is shown in Fig. 1C, in which the 'horizontal' and 'vertical' Fermi surfaces are part of two separate electronic bands). Note that the vicinities of the hot spots in the two-band model are essentially identical to those in the one-band model in Fig. 1A, and so the same low energy theory for the onset of antiferromagnetism applies to both models. With no further assumptions, the deformed model has only positive weights in a suitable quantum Monte Carlo realization.

We will write down a specific lattice model for which we will establish a sign-free Monte Carlo algorithm, and then present numerical results. We begin with the band structure of the $c_{\mathbf{k}}$ electrons in Fig. 1C. We write the band with vertical Fermi surfaces in terms of fermions ψ_x with $c_{\mathbf{k}} \to \psi_{x,\mathbf{k}}$, and the band with horizontal Fermi surfaces in terms of fermions ψ_y with $c_{\mathbf{k}} \to \psi_{y,\mathbf{k+K}}$. This leads to the $\psi_{x,y}$ Fermi surfaces shown in Fig. 2A. Then our model has the

action $S = S_F + S_\varphi = \int_0^\beta d\tau (L_F + L_\varphi)$ with

$$L_F = \sum_{i,j,\alpha=x,y} \psi_{\alpha i}^\dagger \left[(\partial_\tau - \mu) \delta_{ij} - t_{\alpha,ij} \right] \psi_{\alpha j} + \lambda \sum_i \psi_{xi}^\dagger (\vec{s} \cdot \vec{\varphi}_i) \psi_{yi} + H.c.,$$

$$L_\varphi = \frac{1}{2} \sum_i \frac{1}{c^2} \left(\frac{d\vec{\varphi}_i}{d\tau} \right)^2 + \frac{1}{2} \sum_{\langle i,j \rangle} (\vec{\varphi}_i - \vec{\varphi}_j)^2 + \sum_i \left(\frac{r}{2} \vec{\varphi}_i^2 + \frac{u}{4} (\vec{\varphi}_i^2)^2 \right). \tag{2}$$

Here i, j run over the sites of the square lattice, τ is the imaginary time and β - the inverse temperature. The parameter r will be used to tune across the quantum critical point, and u is a non-linear self-coupling of $\vec{\varphi}$. The ψ_x (ψ_y) fermion hops along the horizontal (vertical) direction with an amplitude $t_\parallel = -1 (+1)$, and along the vertical (horizontal) direction with an amplitude $t_\perp = -0.5 (0.5)$, respectively; the resulting band structure is shown in Fig. 2A (solid lines). The model has C_4 symmetry, and its apparent violation is an artifact of the shifting of the ψ_y fermions by $\mathbf{K}$. We chose the chemical potential $\mu_1 = \mu_2 = -0.5$, $c = 1$, $u = 1$, and $\lambda = 1$.

By construction, the modified two-band model has the same hot spot structure as the original one-band model. Therefore, we argue that it preserves the universal properties of the antiferromagnetic transition. We prove (9) that the introduction of the second band eliminates the sign problem in this model.

Note that it is possibly to analytically integrate out $\vec{\varphi}$ in Eq. (S12), and establish equivalence to a large class of Hubbard-like models to which our method applies. However, we choose to keep $\vec{\varphi}$ as in independent degree of freedom because it keeps the physics transparent and streamlines the analysis.

We have performed determinant Monte Carlo simulations of the action (S12) using the algorithm described in Refs. (18–20), for systems of linear size up to $L = 14$ and inverse temperature $\beta = 14$, with either periodic or anti-periodic boundary conditions. An imaginary time step of $\Delta\tau = 0.1$ was used in most of the calculations; we checked that the results do not change for $\Delta\tau = 0.05$. Up to 50000 Monte Carlo sweeps were performed for each run, giving a statistical

error for most measured quantities of a few percent.

First, we present results showing the reconstruction of the Fermi surface across the SDW transition. Fig. 3 shows the fermion occupation number summed over the two flavors of fermions as a function of quasi-momentum. The Fermi surfaces are clearly visible as discontinuities. $r = 0.5$ is found to be on the disordered side of the SDW critical point, and the Fermi surface closely resembles the one in Fig. 2A. At $r = 0$, a gap opens at the hot spots, and the Fermi surface is reconstructed into electron and hole pockets, as in the SDW ordered state in Fig. 2b. Decreasing r further to -0.5 increases the magnitude of the SDW order parameter, and causes the hole pockets to disappear and the electron pockets to shrink.

To examine the magnetic transition, we computed the SDW susceptibility $\chi_\varphi = \sum_i \int_0^\beta d\tau \langle \vec{\varphi}_i(\tau) \cdot \vec{\varphi}_0(0) \rangle$. Figure 4A shows χ_φ normalized by $L^2 \beta$ as a function of r. In order to extract information about the zero-temperature limit, we scale β with the linear system size; in the appropriate units, $\beta = L$ was used. We observe a rapid upturn in χ_φ near $r = 0.25$. For $r < 0.25$, $\chi_\varphi/(L^2\beta)$ for different system sizes and inverse temperatures nearly collapse on top of each other, which is the expected behavior on the ordered side of the transition. The results are consistent with a second-order transition at $r_c \approx 0.25$. This is further supported by the Binder cumulant in Fig. 4B, where we observe the expected behavior in both phases, separated by a critical point at $r_c = 0.25 \pm 0.1$.

The SDW critical modes mediate effective inter-fermion interactions, which can lead to instabilities of the Fermi surface. As a result, additional competing phases can appear. Near the SDW critical point, these instabilities are a result of a subtle competition between the enhancement of the SDW fluctuations, which tends to strengthen the effective interactions, and the loss of coherence of the fermionic quasi-particles (*10, 11*). Superconductivity is a natural candidate for the leading potential instability. In order to examine the emergence of a superconducting phase near the SDW critical point, we have computed equal-time pairing correlations

$P_{\pm}(\vec{x}_i) = \langle \Delta_{\pm}(\vec{x}_i) \Delta_{\pm}(0)^{\dagger} \rangle$. Here, $\Delta_{\pm}(\vec{x}_i) = i s_{ab}^y (\psi_{ixa}\psi_{ixb} \pm \psi_{iya}\psi_{iyb})$ (where $a, b = \uparrow, \downarrow$ are spin indices) are superconducting order parameters with either a $+$ or $-$ relative sign between the two fermionic flavors (square lattice symmetry A_{1g} and B_{1g}, respectively).

In order to probe for long-range order, we measured $P_{\pm}(\vec{x}_i)$ near the maximum range $\vec{x}_{max} = (L/2, L/2)$. We plot $\bar{P}_{\pm}(\vec{x}_{max}) = \frac{1}{9}\sum_{\epsilon_{x,y}=-1}^{1} P_{\pm}(\vec{x}_{max} + \epsilon_x \vec{\eta}_x + \epsilon_y \vec{\eta}_y)$, where $\vec{\eta}_x = (1, 0)$ and $\vec{\eta}_y = (0, 1)$, in Fig. 4C. Long-range superconducting order at $\beta \to \infty$ would correspond to superconducting correlations that saturate to a constant upon increasing L and β.

The B_{1g} pairing correlations are found to be significantly enhanced in the vicinity of the SDW critical point, $r_c \approx 0.25$. The A_{1g} correlations are significantly smaller in magnitude and negative in sign. This is consistent with the expectation that the effective attraction mediated by magnetic fluctuations promotes superconductivity with a sign change between the two orbitals (*22,23*).

The maximum of the B_{1g} correlations occurs for $r \approx 0.5$, on the disordered side of the magnetic critical point which is located at $r_c \approx 0.25$ (*21*). Interestingly, the suppression of the superconducting correlations away from the optimal r is very asymmetric: whereas the pairing correlations decrease gradually for $r > r_c$, they are suppressed dramatically for $r < r_c$. This may be a result of the opening of an SDW gap on portions of the Fermi surface.

The method described in this Letter opens the way to study various physical aspects of spin density wave transitions in metals, in a numerically exact way. The interplay between unconventional superconductivity and magnetism and possible non-Fermi liquid behavior in the quantum critical regime should now be accessible. Moreover, such simulations will provide controlled benchmarks for analytic approximations (*7,8,10,11*).

The two-band model presented here is a member of a wider family of strongly correlated fermionic models that can be rendered free of the sign problem. It has already been known that some models with two flavors of fermions interacting via a four-fermion interaction are sign

problem free at generic fermion density (*24*). Remarkably, these models do not rely on any specific characteristic of the electron dispersion; e.g. there is no requirement for particle-hole symmetry, or any symmetry that relates the two bands. Extensions of this trick to related models of physical interest should be possible.

References and Notes

1. T. Helm *et al.*, Magnetic Breakdown in the Electron-Doped Cuprate Superconductor $Nd_{2-x}Ce_xCuO_4$: The Reconstructed Fermi Surface Survives in the Strongly Overdoped Regime, M. V. Kartsovnik, I. Sheikin, M. Bartkowiak, F. Wolff-Fabris, N. Bittner, W. Biberacher, M. Lambacher, A. Erb, J. Wosnitza, and R. Gross, Phys. Rev. Lett. **105**, 247002 (2010).

2. K. Hashimoto *et al.*, A Sharp Peak of the Zero-Temperature Penetration Depth at Optimal Composition in $BaFe_2(As_{1-x}P_x)_2$, Science **336**, 1554 (2012).

3. T. Park *et al.*, Hidden magnetism and quantum criticality in the heavy fermion superconductor $CeRhIn_5$, Nature **440**, 65 (2006).

4. L. Balents, Spin liquids in frustrated magnets, Nature **464**, 199 (2010).

5. M. Troyer and U.-J. Wiese, Computational complexity and fundamental limitations to fermionic quantum Monte Carlo simulations, Phys. Rev. Lett. **94**, 170201 (2005).

6. J. A. Hertz, Quantum critical phenomena, Phys. Rev. B **14**, 1165 (1976).

7. Ar. Abanov and A. V. Chubukov, Spin-Fermion Model near the Quantum Critical Point: One-Loop Renormalization Group Results, Phys. Rev. Lett. **84**, 5608 (2000).

8. Ar. Abanov and A. V. Chubukov, Anomalous Scaling at the Quantum Critical Point in Itinerant Antiferromagnets, Phys. Rev. Lett. **93**, 255702 (2004).

9. See Supplementary Material.

10. M. A. Metlitski and S. Sachdev, Quantum phase transitions of metals in two spatial dimensions. II. Spin density wave order, Phys. Rev. B **82**, 075128 (2010).

11. S. A. Hartnoll *et al*., Quantum critical response at the onset of spin-density-wave order in two-dimensional metals Phys. Rev. B **84**, 125115 (2011).

12. C. Weber, K. Haule, and G. Kotliar, Apical oxygens and correlation strength in electron- and hole-doped copper oxides, Phys. Rev. B **82**, 125107 (2010).

13. L. Taillefer, Scattering and Pairing in Cuprate Superconductors, Annual Review of Condensed Matter Physics **1**, 51 (2010)

14. N. Doiron-Leyraud and L. Taillefer, Quantum critical point for stripe order: An organizing principle of cuprate superconductivity, Physica C **481**, 161 (2012).

15. G. Sordi, P. Sémon, K. Haule, and A.-M. S. Tremblay, Strong Coupling Superconductivity, Pseudogap, and Mott Transition, Phys. Rev. Lett. **108**, 216401 (2012).

16. E. Gull, O. Parcollet, and A. J. Millis, Superconductivity and the Pseudogap in the two-dimensional Hubbard model, arXiv:1207.2490.

17. Ar. Abanov, A. V. Chubukov, and J. Schmalian, Quantum-critical theory of the spin-fermion model and its application to cuprates: Normal state analysis, Advances in Physics **52**, 119 (2003).

18. R. Blankenbecler, D. J. Scalapino, and R. L. Sugar, Monte Carlo calculations of coupled boson-fermion systems, Phys. Rev. D **24**, 2278 (1981).

19. S. R. White *et al*., Numerical study of the two-dimensional Hubbard model, Phys. Rev. B **40**, 506 (1989).

20. F. F. Assaad and H. G. Evertz, World-line and Determinantal Quantum Monte Carlo Methods for Spins, Phonons and Electrons, in *Computational Many-Particle Physics*, H. Fehske, R. Shnieider, and A. Weiße Eds., Springer, Berlin (2008).

21. E. G. Moon and S. Sachdev, Quantum critical point shifts under superconductivity: Pnictides and cuprates, Phys. Rev. B **82**, 104516 (2010).

22. D. J. Scalapino, E. Loh, and J. Hirsch, d-wave pairing near a spin-density-wave instability, Phys. Rev. B **34**, 8190 (1986).

23. P. Monthoux, A. Balatsky, and D. Pines, Toward a theory of high-temperature superconductivity in the antiferromagnetically correlated cuprate oxides, Phys. Rev. Lett. **67**, 3448 (1991).

24. Y. Motome and M. Imada, A Quantum Monte Carlo Method and Its Applications to Multi-Orbital Hubbard Models, J. Phys. Soc. Jpn. **66**, 1872 (1997).

25. I. F. Herbut, V. Juricic, and O. Vafek, Relativistic Mott criticality in graphene, Phys. Rev. B **80**, 075432 (2009).

26. S. Capponi, C. Wu, and S.-C. Zhang, Current carrying ground state in a bilayer model of strongly correlated systems, Phys. Rev. B **70**, 220505(R) (2004).

27. C. Wu and S.-C. Zhang, Sufficient condition for absence of the sign problem in the fermionic quantum Monte Carlo algorithm, Phys. Rev. B **71**, 155115 (2005).

28. We thank F. Assaad, D. Chowdhury, H. Evertz, S. Kivelson, T. Lang, J.-Y. Lee, M. Punk, and P. Strack for discussions. This research was supported by the NSF under Grants DMR-1103860, DMR-0705472, and PHY11-25915, by the ISF under Grant No. 433117, and by a MURI grant from AFOSR. The computations were run on the Odyssey cluster supported by the FAS Science Division Research Computing Group at Harvard University.
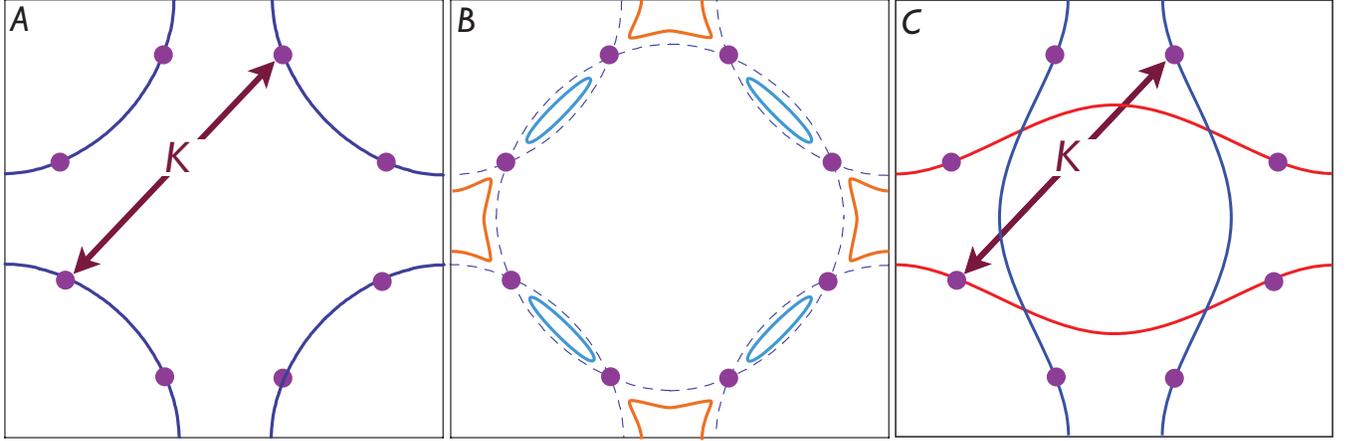
Figure 1: (*A*) Fermi surface of the Fermi liquid phase of a single band model on the square lattice with unit lattice spacing. The "hot spots" are denoted by the filled circles. (*B*) The reconstructed Fermi surface in the metal with SDW order. The dashed lines show the Fermi surface in the metal without SDW order, and its translation by **K**. Gaps have opened at the hot spots, leading to small "pocket" Fermi surfaces. (*C*) A deformed Fermi surface of the metal without SDW order, in which the vicinities of the hot spots are unchanged from (A). The horizontal and vertical Fermi surfaces now belong to separate electronic bands.
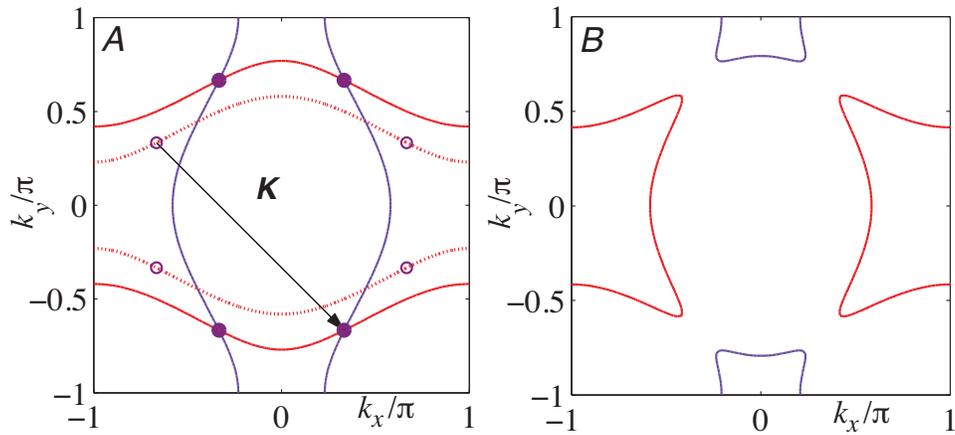

Figure 2: (*A*) Fermi surfaces (full lines) of L_F for free $\psi_{x,y}$ fermions with the parameters listed in the text. The dashed lines show the portion of the Fermi surface in Fig. 1c which was shifted by **K** to obtain the ψ_y Fermi surface. Now the hot spots are at the intersections of the Fermi surfaces. (*B*) Mean-field $\psi_{x,y}$ Fermi surfaces with SDW order $|\langle \vec{\varphi} \rangle| = 0.25$.
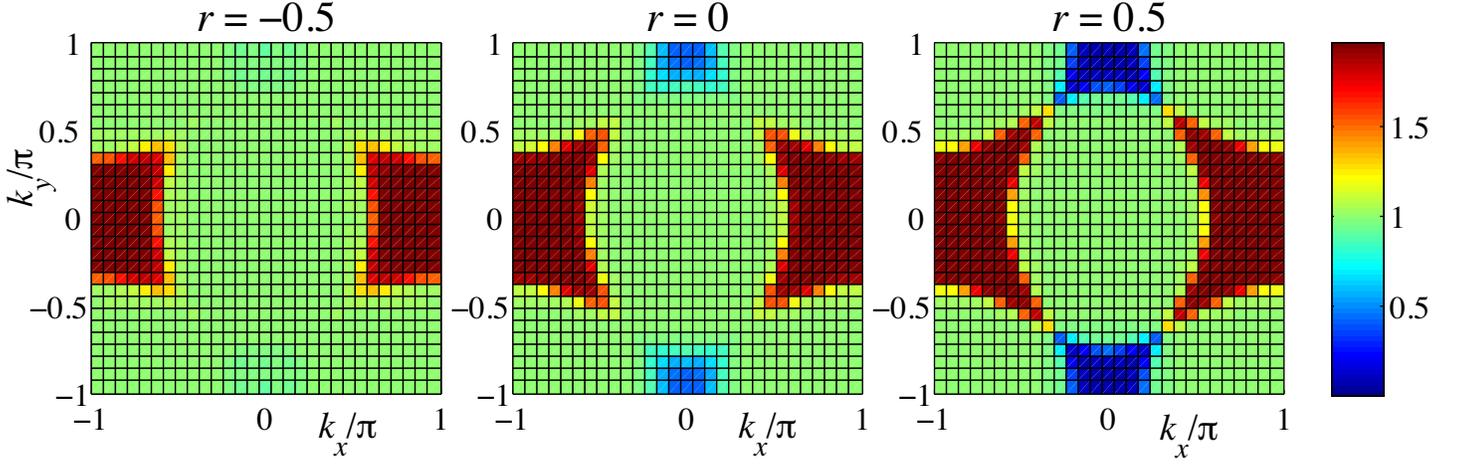
12

Figure 3: Quantum Monte-Carlo results for the fermion occupation number $n_{\mathbf{k}} = \langle \psi^\dagger_{x\mathbf{k}}\psi_{x\mathbf{k}} + \psi^\dagger_{y\mathbf{k}}\psi_{y\mathbf{k}}\rangle/2$ as a function of $\mathbf{k}$ across the Brillouin zone, for systems with $L = 14$, $\beta = 14$, and $r = -0.5, 0, 0.5$. In order to enhance the resolution, results from simulations with either periodic or anti-periodic boundary conditions in the x and y directions were combined. Despite appearances, full square lattice symmetry is preserved in all our computations for the original $c_{\mathbf{k}}$ fermions.
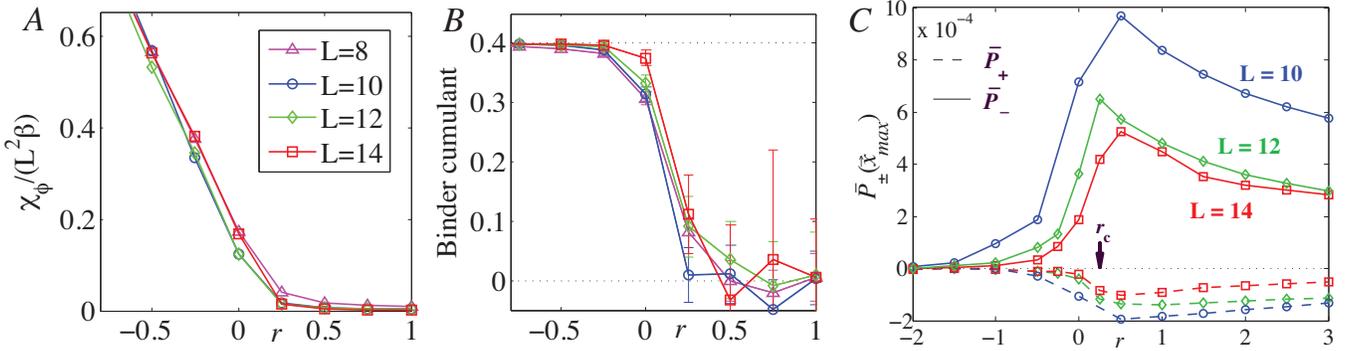

Figure 4: (*A*) The SDW susceptibility χ_φ, normalized by $L^2\beta$, as a function of r, for systems of size $L = 8, 10, 12, 14$ and $\beta = L$ for each curve. The statistical errors in χ_ϕ are smaller than the symbol size. (*B*) The Binder cumulant for an O(3) order parameter $C_B = 1 - \frac{3\langle\vec{\Phi}^4\rangle}{5\langle\vec{\Phi}^2\rangle^2}$, where $\vec{\Phi} = \frac{1}{\mathcal{N}}\sum_i \vec{\varphi}_i$, approaching the expected values of 0.4 and 0 in the two phases. (*C*) Equal-time pairing correlations in systems of size $L = 10, 12, 14$ and $\beta = L$ for each curve, as a function of r. Dashed (solid) lines show $\bar{P}_+$ ($\bar{P}_-$), corresponding to A_{1g} (B_{1g}) superconducting order parameters, in which the pairing amplitude in the two fermion flavors is of the same (opposite) sign, respectively. r_c is the estimated position of the SDW critical point.

Supplementary Material

Quantum Field Theory

In this section, we briefly review the universal field theory for the SDW transition developed in Refs. (*7,8,10,11*). This effective field theory has been analyzed perturbatively in the order parameter-fermion coupling λ.

One of the key results of the analysis is that, if we ignore the possibility of a high-energy pairing instability, the fermion and order parameter propagators acquire *universal* singular parts which depend only on the structure of the hot spots (e.g. the velocities at the hot spots and the angle between them). This justifies the assumptions behind the construction of the lattice model presented in the main text: as long as the structure of the hot spots is preserved, we expect the universal behavior near the antiferromagnetic critical point to be unchanged. The microscopic parameters of the model should only come in through the ultraviolet cutoffs to the critical fluctuations. These cutoffs can, in principle, be set by matching at high energy scales. Specifically, we can match a sign-problem-free lattice model to a Hubbard-like model by equating their hot-spot Fermi surfaces and Fermi velocities. Other parameters of the sign-problem-free model can be determined by matching its physical observables to those of the sign-problem-present Hubbard model at temperatures high enough to allow accurate computations by other methods for the latter model. The sign-problem-free model can then be used to compute observables at low temperatures.

Another observation made in Ref. (*10*), however, is that ultimately the conventional ways to control the perturbative series for the effective field theory, such as an expansion in the inverse number of fermion flavors, are uncontrolled for this problem. The fate of the flow to strong coupling has to be resolved by numerical simulations. For this we need a lattice regularization of the continuum quantum field theory, and the lattice model considered in the main body of the

paper provides precisely such a regularization.

The field theory is formulated in terms of the fermion excitations in the vicinity of the hot spots. The antiferromagnetic order parameter $\vec{\varphi}$, with wavevector $\mathbf{K}$, connects fermions at a hot spot at wavevector $\mathbf{k}$ with fermions at a hot spot with wavevector $\mathbf{k} + \mathbf{K}$; both fermions are on the Fermi surface if $\varepsilon_{\mathbf{k}} = \varepsilon_{\mathbf{k}+\mathbf{K}} = 0$, and this defines the allowed values of $\mathbf{k}$. Linearizing the fermion dispersion about the hot spots, and expanding the order parameter in spatial gradients, in two spatial dimensions we obtain the Lagrangian $L = L_{\psi} + L_{\varphi}$ where

$$
\begin{aligned}
\mathcal{L}_{\psi} &= \psi_1^{\dagger} \left(\partial_{\tau} - i\mathbf{v}_1 \cdot \nabla \right) \psi_1 + \psi_2^{\dagger} \left(\partial_{\tau} - i\mathbf{v}_2 \cdot \nabla \right) \psi_2 + \lambda \vec{\varphi} \cdot (\psi_1^{\dagger} \vec{s} \psi_2 + \text{H.c.}) \\
\mathcal{L}_{\varphi} &= \frac{1}{2c^2}(\partial_{\tau}\vec{\varphi})^2 + \frac{1}{2}(\nabla\vec{\varphi})^2 + \frac{r}{2}\vec{\varphi}^2 + \frac{u}{4}(\vec{\varphi}^2)^2
\end{aligned}
\tag{S1}
$$

Here ψ_a, with $a = 1, 2$, are two species of low energy fermions in the vicinity of the hot spots at $\mathbf{k}$ and $\mathbf{k} + \mathbf{K}$, and $\mathbf{v}_a$ are their Fermi velocities. A similar Lagrangian applies to the other hot spots. This theory has the same general structure as coupled fermion-boson theory in particle physics, such as the Gross-Neveu model (25), with fermions and bosons coupled via trilinear "Yukawa" coupling λ. The key difference is in the fermion dispersion, which does not have a relativistic form. In the relativistic cases, the fermion dispersion has a Dirac form with energy $\sim \pm v|\mathbf{k}|$, and this vanishes only at isolated points in the Brilluoin zone. The resulting fermion-boson theory is well understood (25). In our case, the fermions dispersion $\sim \mathbf{v} \cdot \mathbf{k}$, and this vanishes on a *line* in the Brillouin zone which is orthogonal to $\mathbf{v}$. This is the central difference which makes the quantum field theory in Eq. (S1) strongly coupled.

Let us parametrize the Fermi velocities by

$$
\mathbf{v}_1 = (v_x, v_y), \qquad \mathbf{v}_2 = (-v_x, v_y).
\tag{S2}
$$

Here, for convenience, we have rotated the coordinates by $45°$ relative to Fig. 1a in the main text. It is useful to introduce the ratio and the modulus

$$
\tan\phi \equiv \frac{v_y}{v_x}, \qquad v = |\mathbf{v}|.
\tag{S3}
$$

Here $0 < 2\phi < \pi$ is the angle between the Fermi surfaces at the hot spot. We now present the singular terms in the low energy spectrum at two loop order, as obtained in Refs. (*10,17*). We will restrict the expressions to precisely at the quantum critical point at zero temperature; all our conclusions, and similar but lengthier expressions, apply also close to the quantum critical point and at low temperatures. For the fermion Green's function we have

$$G_a^{-1}(\omega, \mathbf{p}) = -\mathbf{v}_a \cdot \mathbf{p} + \frac{3v \sin 2\phi}{8} i \, \mathrm{sgn}(\omega) \left(\sqrt{\gamma|\omega| + \frac{(\mathbf{v}_{\bar{a}} \cdot \mathbf{p})^2}{v^2}} - \frac{|\mathbf{v}_{\bar{a}} \cdot \mathbf{p}|}{v} \right), \qquad (\text{S4})$$

where ω is an imaginary frequency, $\bar{1} = 2$ and $\bar{2} = 1$, and

$$\gamma = \frac{N_h \lambda^2}{2\pi v_x v_y}, \qquad (\text{S5})$$

where N_h is the number of pairs of hot spots ($N_h = 4$ for the electron-doped cuprates). In the expression (S4) we have dropped the bare free fermion $i\omega$ term because it is not as singular as the self-energy correction from the fluctuations of the antiferromagnetic order, and we have not explicitly written the real part of the self energy which renormalizes the velocities v_x and v_y. The singular part of the propagator of the boson $\vec{\varphi}$ is

$$D^{-1}(\omega, \vec{p}) = \gamma|\omega| + \mathbf{p}^2. \qquad (\text{S6})$$

In these expressions above the strength of the interactions is controlled by the Yukawa coupling λ, and hence via the value of γ. However a key observation is that dependence on λ can be scaled away, and the above low energy spectra are actually universal. Indeed, it is easily seen from Eqs. (S4,S6) that after rescaling momenta by $\mathbf{p} \to \lambda \mathbf{p}$, the λ dependence appears as overall prefactors which can be absorbed into a rescaling of the fields. This independence on the value of λ is a general feature of the low-energy quantum field theory (*10*), and is crucial to its properties. One of its consequences appeared in the leading log estimate of the pairing instability presented in Ref. (*10*), which was found to be a logarithm-squared term with a λ-independent prefactor.

Quantum Monte Carlo

We set up $S_F + S_\varphi$ for a Monte Carlo study (*17*). Discretizing imaginary time, the partition function becomes

$$Z = \int d\varphi \exp\left(-S_\varphi\right) \mathrm{Tr}_\psi \left[\prod_{n=1}^{N} \hat{B}_n\right] + O\left(\Delta\tau^2\right), \tag{S7}$$

where $\Delta\tau$ is an imaginary time step, $\beta = N\Delta\tau$, and the operators $\hat{B}_n$ are given by

$$\hat{B}_n = e^{-\frac{1}{2}\Delta\tau\psi^\dagger K\psi} e^{-\Delta\tau\psi^\dagger V_n\psi} e^{-\frac{1}{2}\Delta\tau\psi^\dagger K\psi}. \tag{S8}$$

K and V_n are matrices given by

$$K_{i,j;\alpha,\alpha';s,s'} = \delta_{s,s'}\delta_{\alpha,\alpha'}\left(-t_{\alpha,ij} - \mu\right)$$

$$V_{n;i,j;\alpha,\alpha';s,s'} = \lambda\left(\sigma_1\right)_{\alpha,\alpha'} \delta_{ij} \left[\vec{s}\cdot\vec{\varphi}_i\left(n\Delta\tau\right)\right]_{s,s'}, \tag{S9}$$

where i, j are spatial indices, σ_1 is a Pauli matrix, $\alpha, \alpha' = x, y$ are flavor indices, and $s, s' = \uparrow, \downarrow$ are spin indices. $\psi^\dagger$ is a vector of fermionic operators,

$$\psi^\dagger = \left(\psi^\dagger_{x,1,\uparrow}, \ldots, \psi^\dagger_{x,\mathcal{N},\uparrow}, \psi^\dagger_{x,1,\downarrow}, \ldots, \psi^\dagger_{x,\mathcal{N},\downarrow},\right.$$

$$\left.\psi^\dagger_{y,1,\uparrow}, \ldots, \psi^\dagger_{y,\mathcal{N},\uparrow}, \psi^\dagger_{y,1,\downarrow}, \ldots, \psi^\dagger_{y,\mathcal{N},\downarrow}\right). \tag{S10}$$

$\mathcal{N}$ is the number of lattice sites. Note that Tr_ψ in Eq. S7 represents a trace over fermionic many-body states in Fock space. This fermionic trace can be carried out, giving

$$\mathrm{Tr}\left[\prod_{n=1}^{N} \hat{B}_n\right] = \det\left[1 + \prod_{n=1}^{N} B_n\right], \tag{S11}$$

where $B_n = e^{-\frac{1}{2}\Delta\tau K} e^{-\Delta\tau V_n} e^{-\frac{1}{2}\Delta\tau K}$. For a proof of this formula, see, e.g., Ref. (*19*). We then arrive at the following form of the partition function:

$$Z = \int d\varphi \exp\left(-S_\varphi\right) \det\left[1 + \prod_{n=1}^{N} B_n\right] + O\left(\Delta\tau^2\right), \tag{S12}$$

which can be evaluated using Monte Carlo techniques, by sampling over space-time configurations of $\vec{\varphi}_i\left(\tau\right)$.

Positivity of the action

Monte Carlo sampling can be done efficiently if the action in Eq. S12 is non-negative. To show that this is the case, we note that the matrix

$$M\left[\vec{\varphi}\right] \equiv 1 + \prod_{n=1}^{N} B_n \tag{S13}$$

commutes with the following anti-unitary operator:

$$\mathcal{U} = i s_2 \sigma_3 K, \tag{S14}$$

where $\vec{s}$ are Pauli matrices which act on the spin index, $\vec{\sigma}$ are Pauli matrices which act on the orbital (x, y) index, and K is the complex conjugation operator. Note that $\mathcal{U}^2 = -1$. Using this, one can prove (*26,27*) (in a similar way to the proof of Kramers' theorem) that if λ_α is an eigenvalue of M, λ_α^* is an eigenvalue also, and that if λ_α is real then it is doubly degenerate. The determinant can be written as $\det\left[M\right] = \prod_\alpha |\lambda_\alpha|^2 \geq 0$. The integrand in the partition function (Eq. S12) is therefore non-negative, and can be simulated using Monte Carlo without a sign problem. Note that there are no particular restrictions on t_{ij} (*e.g.* it does not have to be bipartite) or μ. So particle-hole symmetry or specific densities are not required.